FINAL PROJECT REPORT FOR EUROPAN SCIENCE FOUNDATION PROGRAMME (ORGANISOLAR)

Organic bulk heterojunction and bilayer solar cells employing liquid crystalline n-type perylene bisimides

Grantee: André Wicklein, Makromolekulare Chemie I, Applied Functional Polymers, University of Bayreuth, Germany

Host: Dr. Neil Greenham, Cavendish Laboratory, University of Cambridge, United Kingdom

1. Purpose of the visit

1.1 Introduction

Perylene bisimide ("perylenetetracarboxdiimide", PBI) derivatives represent an important class of organic n-type semiconductor materials exhibiting a relatively high electron affinity among large-band-gap materials. They are promising candidates for application in organic electronic devices.[1] The solid-state packing of the perylene bisimide derivatives plays a major role in improving the device performance. For instance an increase in exciton diffusion length and an improvement in charge carrier mobility can be achieved by increased ordering of perylene molecules.[2,3] Inducing liquid crystallinity is an elegant way of improving organization because it promotes π-π stacking, allows for dynamic reorganization, and facilitates the processing of thin films, which is not feasible with organic single crystals or insoluble compounds. We recently synthesized highly soluble, unsymmterically *N*-substituted perylene bisimide

derivatives bearing branched alkyl chains and branched oligoethyleneglycolethers[4] (Figure 1).

1.2 Aim of the study

The aim of the visit to Neil Greenhams group at Cavendish Laboratory in Cambridge is to elucidate the potential of liquid crystalline perylene bisimides (PBIs) in organic electronic devices like photovoltaic cells or field effect transistors (OFET). Due to the hexagonal columnar liquid crystalline behavior of the involved n-type semiconducting dyes, an enhanced charge carrier mobility in the mesophase is expected. This effect should be proven directly in devices. Thus photovoltaic devices employing liquid crystalline perylene bisimides in combination with suitable hole conducting materials should be prepared and fully characterized by current-voltage characteristics and external quantum efficiency spectra. By using different processing methods and thermal annealing conditions, the influence on thin-film morphology and the liquid crystalline ordering on device performance will be studied. As hole transport material (HTM), a focus was set on conjugated polymers, like *poly*(3-hexylthiophene) (p3HT) or amorphous *p*vDMTPD (*poly*(vinyl-dimethoxytetraphenylbenzidine)) but also low molecular copper phthalocyanine (CuPc) pigments (Scheme X).

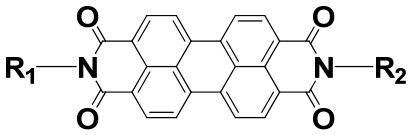

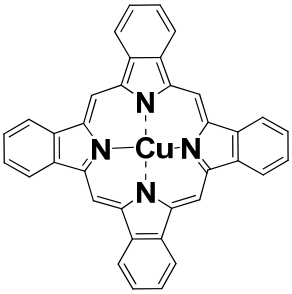

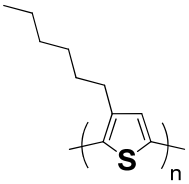

PBI1: $R_1 = R_2 = -CH(CH_2CH_2CH_2CH_2CH_2CH_2CH_3)_2$ **CuPc** **p3HT**

PBI2: $R_1 = -CH(CH_2CH_2CH_2CH_2CH_2CH_2CH_3)_2$
$R_2 = -CH(CH_2OCH_2CH_2OCH_2CH_2OCH_3)_2$

PBI3: $R_1 = R_2 = -CH(CH_2OCH_2CH_2OCH_2CH_2OCH_2CH_2OCH_3)_2$

Scheme 1. Chemical structures of perylene bisimides PBI1-3, copper phthalocyanine (CuPc) and *poly*(3-hexylthiophene) (p3HT).

In the case of CuPc as HTM, thin-film bilayer heterojunction photovoltaic devices will be constructed. CuPc can be deposited by physical vapour deposition. Due to high

solubility of the perylene bisimides, even in polar solvents, perylene bismide can be processed by solution techniques (spin-coating or doctor-blading) on top of CuPc. As CuPc is a high melting pigment, the upper liquid-crystalline PBI layer can easily be thermally annealed. Employing perylene bisimides in combination with p3HT as HTM, one can compare the difference in device performance of a blend (different compositions) cell with a bilayer device that can be prepared by using an orthogonal solvent system for processing of the individual layers. This comparison allows for conclusions about the factors influencing device efficiency. Thus, the following device architectures will be investigated:

Bilayer cells: ITO/PEDOT:PSS/CuPc/Col_h-PBI/Ag
ITO/PEDOT:PSS/p3HT/Col_h-PBI/Al
Blend cells: ITO/PEDOT:PSS/p3HT:Col_h-PBI blends/LiF/Al.

Also an investigation of the temperature dependence of the charge carrier mobility in the different phases (crystalline versus columnar hexagonal liquid crystalline mesophase) of the selected compounds is of great interest. To this end organic field effect transistors (OFETs) should be prepared and characterized temperature dependently.

The relative orientation of the discotic PBIs with respect to the substrate surface is a fundamental question in electronic devices. For photovoltaic devices, a face-on orientation (homeotropic) of the chromophores is the desired one (Fig. 1a). In contrast, in field-effect transistors, an edge-on orientation of the columns, spanning the gap between source and drain electrodes is favored. [5]

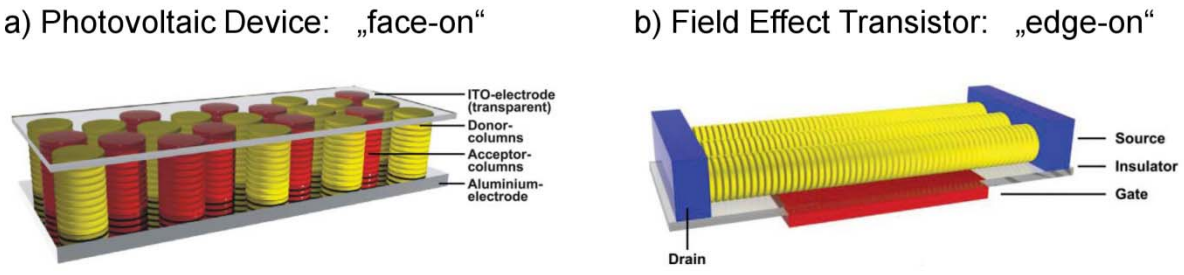

Figure 1. Schematic representation of the desired arrangement of discotic molecules as electronically active components with an a) face-on orientation for photovoltaic devices and b) edge-on orientation for OFETs.

2. Photovoltaic Devices employing Col_h-PBI

2.1 Experimental Section

Precleaned ITO-substrates were exposed to oxygen-plasma (250 Watt) for 10 minutes. A filtered suspension of PEDOT:PSS (poly(3,4-ethylenedioxythiophene): poly(styrenesulfonate) from Cambridge Display Technology Ltd.) in water was spin coated at 4000 rpm for 60 s onto the ITO-substrates. The films were cured by heating on a temperature-controlled hot plate at 150 °C for 30 minutes under N_2-atmosphere. All subsequent steps, processing of active layers and annealing processes were performed under a N_2-atmosphere in a glovebox (see respective discussion section for further details). The metal cathodes (Al or Ag) were deposited through a shadow mask in a thermal evaporator at a base pressure of $2x10^{-6}$ mbar to a thickness of 100 nm. The configuration of the shadow mask ensured 8 independent devices on each substrate, each with an active area of 1.5 x 4.0 mm. The devices were then “legged” to allow electrical connection and encapsulated in glass using an epoxy resin and hardener (Robnor Resins Ltd., UK), without the need for additional thermal annealing. The devices were tested at room temperature, under illumination from a calibrated thermal white-light source and monochromator, using a Keithley 195 DMM system parameter analyzer and a Keithley 237 source measure unit. The illumination source was focused down to a spot size of ~1 mm^2. Films for optical spectroscopy and AFM were prepared under the same conditions as those used for solar cell preparation on spectrosil® quartz substrates. Tapping-mode atomic force micrographs were taken with a Veeco Nanoscope IIIa instrument. UV-vis absorption measurements were performed on a Hewlett-Packard 8453 spectrophotometer

2.2 Experiments on CuPc Col_h-PBI bilayer heterojunction devices

In this study we wanted to investigate the effect of the liquid crystalline phase of PBI2 on the performance in photovoltaic devices. According to DSC measurements, PBI2 enters the hexagonal-columnar mesophase (Col_h) at 66 °C upon heating and the isotropic phase at 149 °C. Upon cooling PBI3 orientates againg into the Col_h-phase at 142 °C and no crystallization can be observed upon further cooling. This gives the

possibility to freeze-in the desired morphology. We first used a very simple system, which allows solution processing of the PBIs without affecting the insoluble underlying CuPc pigment layer. Photovoltaic devices employing either a crystalline perylene bisimide PBI1, as reference, or Col_h PBI3 as n-type material in combination with copper phthalocyanine (CuPc) pigment as p-type material were prepared. The used bilayer heterojunction device configuration (ITO/PEDOT:PSS/CuPc (30 nm)/PBI/Ag) and the corresponding energy diagram are shown in Figure 2. This device setup is also beneficial for studying different annealing procedures of the perylene bisimide dye in the mesophase temperature range.

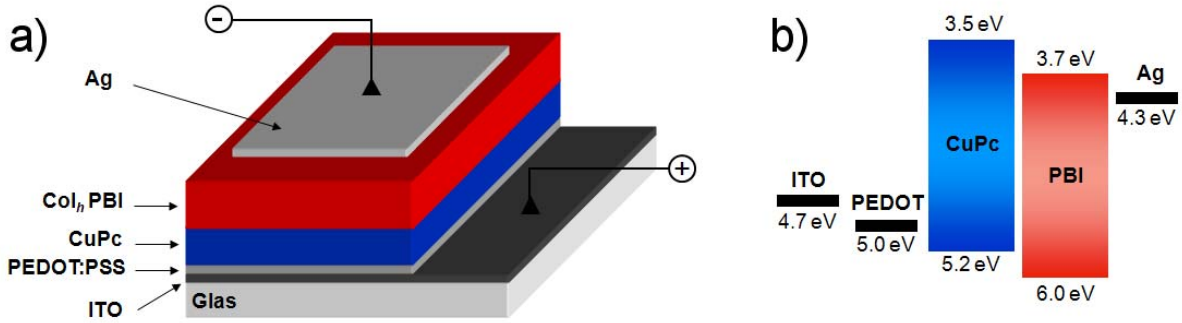

Figure 2. (a) Device architecture for CuPc-PBI bilayer devices. **(b)** Hypothesized energy diagram of ITO/PEDOT:PSS/CuPc/Col_h-PBI/Ag devices.

The CuPc pigment was previously purified by train sublimation and was deposited by thermal evaporation through a shadow mask at about $2x10^{-6}$ mbar, at 340 °C and a deposition rate of 0.1–0.2 $Å s^{-1}$. The PBI layers were processed by spin coating from $CHCl_3$ (10 mg/mL) solutions on top of CuPc and were used as spun or after annealing at 80 °C for 1 h. The UV-vis absorption spectra of CuPc/PBI2 bilayer film is a superposition of the individual absorption spectra (Fig. 3). The combination of CuPc pigments with PBI dyes guarantees efficient light harvesting in the range of 400 up to 800 nm, covering the completely the visible spectral region.

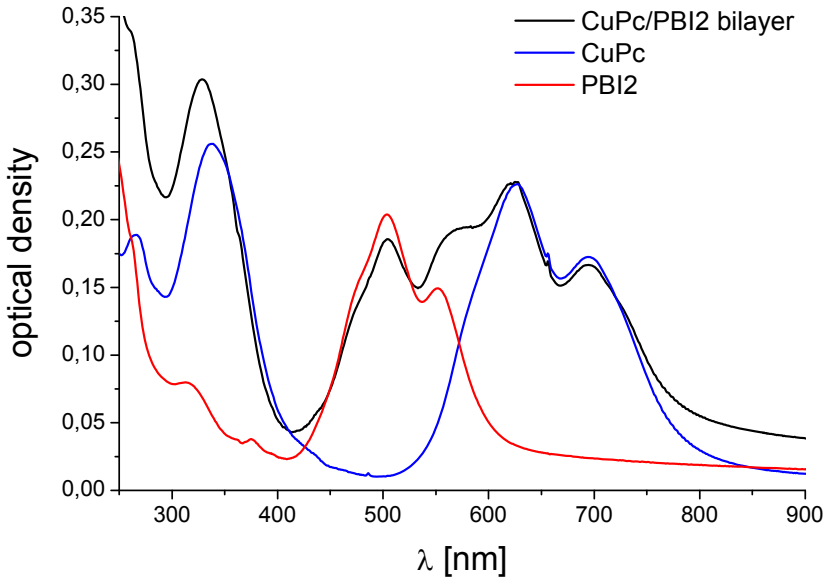

Figure 3. UV-vis absorption spectra of individual PBI2, CuPc and CuPc/PBI2 bilayer films.

Figure 4 shows AFM height and phase images of the CuPc/PBI2 bilayer films and pure PBI2 films. PBI2 covers the surface of the CuPc layer completely without. The PBI2 morphology is highly dependent on the annealing conditions and the underlying layer. On top of CuPc, PBI2 forms a multicrystalline layer (Fig. 4a, d) which changes its morphology drastically upon annealing at 80 °C (Fig. 4b, e). In contrast to the crystalline PBI2 layer formed on CuPc, PBI2 forms fiber-like aggregates on quartz substrates (Fig. 4c, f).

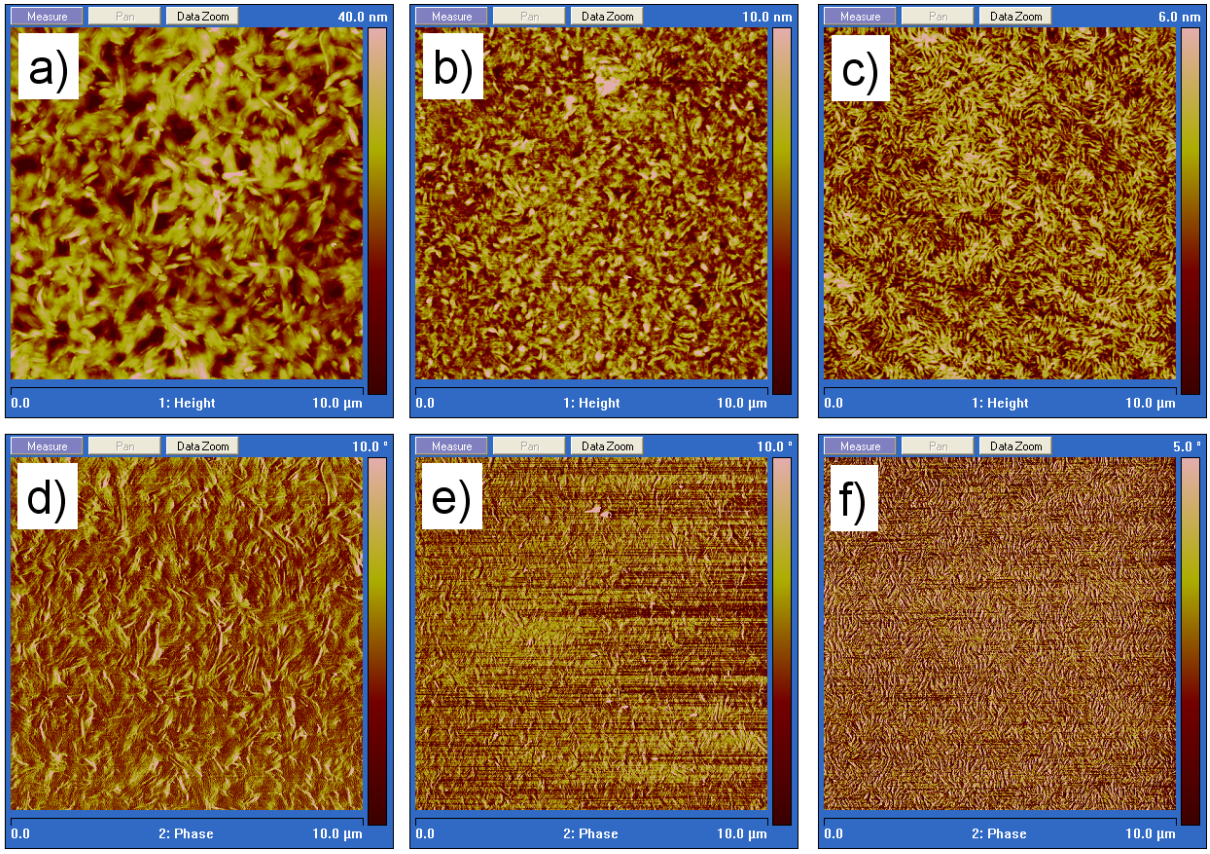

Figure 4. (a) AFM height image of PBI2 on CuPc (as spun) and (d) corresponding phase image. (b) AFM height image of PBI2 on CuPc (after annealing at 80 °C for 1 h) and (e) corresponding phase image. (c) AFM height image of AW96 on quartz (after annealing at 80 °C for 1 h) and (f) corresponding phase image.

Due to overlapping problems of the shadow mask with the ITO-stripe on the substrates, as prepared devices were all short-circuited and over the time period of the project no further devices could be prepared.

2.3 Experiments on p3HT Col$_h$-PBI bilayer heterojunction devices

PBI3 with two polar, swallow-tailed substituents is soluble in alcohols and is therefore optimally suited for preparing bilayer devices by using an orthogonally solvent system. According to DSC measurements, PBI3 enters the hexagonal-columnar mesophase (Col$_h$) at 68 °C upon heating and the isotropic phase at 127 °C. Upon cooling PBI3 orientates againg into the Col$_h$-phase at 121 °C and no crystallization can be observed upon further cooling. This gives the possibility to freeze-in the desired morphology. In these experiments devices of the following architecture were prepared: ITO/PEDOT:PSS/p3HT/PBI3/Al (Fig. 5a). Figure 5b shows the hypothesized energy diagram of such a device with the corresponding HOMO/LUMO values of the materials. The p3HT layer was annealed in all devices and the subsequent PBI3 layer was used as spun or after annealing in the liquid crystalline phase shortly before isotropic phase transition temperature T_{iso} = 127 °C in order to study the effect of the liquid crystallinity of PBI3. Solutions of p3HT were prepared in chlorobenzene (PhCl) or *o*-xylene at a concentration of 15 mgmL^{-1} and spin coated on top of the PEDOT:PSS layer. The p3HT layers were annealed at 150 °C for 10 minutes. Layers of PBI3 were prepared by spin coating from hot (80 °C) 1.0 or 3.0 wt-% isopropanol (IPA) solutions as orthogonal solvent system. In devices, the PBI3 layers were annealed at 120 °C for one hour, followed by slow cooling to room temperature, or used as spun.

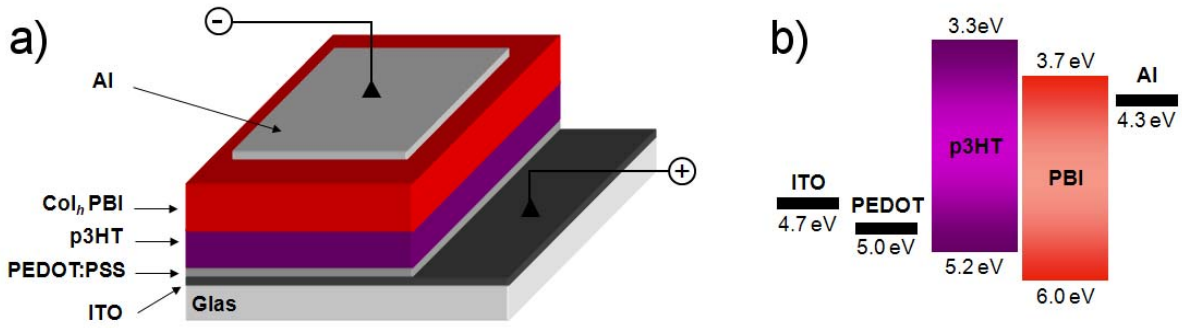

Figure 5. (a) Device architecture for p3HT-PBI bilayer devices. **(b)** Hypothesized energy diagram of ITO/PEDOT:PSS/p3HT/Col$_h$-PBI/Al devices.

The UV-vis absorption spectra of the p3HT/PBI3 bilayer film is a superposition of the individual absorption spectra (Fig. 6). The absorption maximum of PBI3 at 470 nm indicates a strong aggregation of the chromophores.

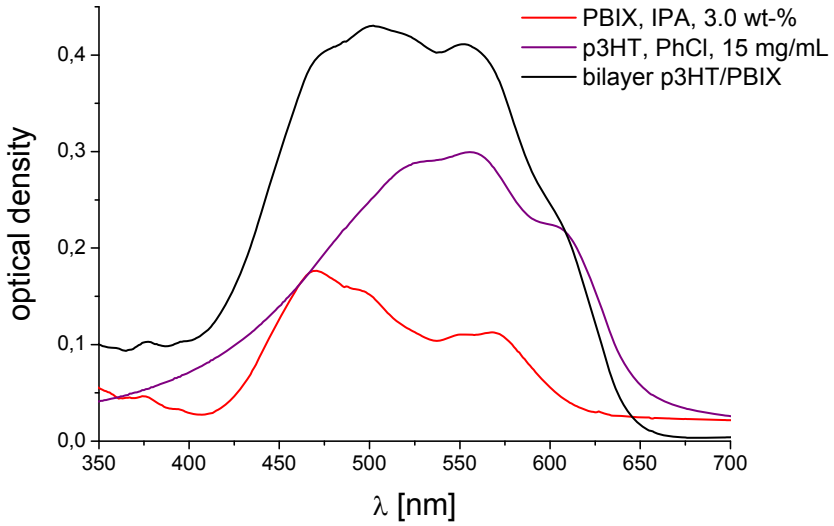

Figure 6. UV-vis absorption spectra of individual PBI3 and p3HT layers and p3HT/PBI3 bilayer films.

Figure 7 shows AFM height and phase images of the p3HT/PBI3 bilayers (as spun). PBI3 covers the whole surface of the p3HT film and forms thin schist-like aggregates. These aggregates are lying planar or side-on orientated on the p3HT film. Figure 7c shows a surface cross section of PBI3 on CuPc film. The step-heights of the aggregates are approximately 1.6 - 1.8 nm. These values are corresponding to the intercolumnar layer spacing (d_{100} = 18.02 Å) of PBI3 columns, as determined from XRD-measurements, and thus indicate a side-on orientations of PBI3 columns on the p3HT surface.

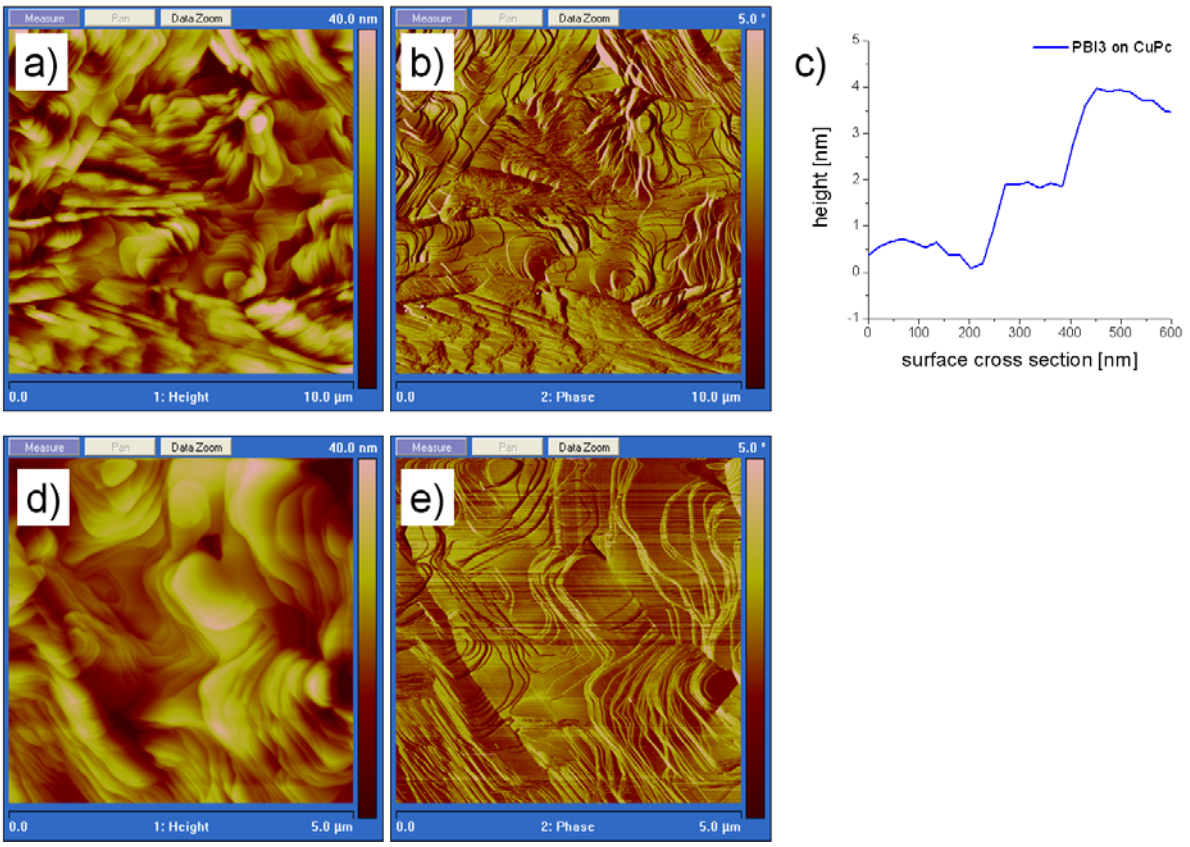

Figure 7. AFM height (a, b) and phase (d, e) images of p3HT/PBI3 bilayer. (c) Surface cross section of PBI3 on CuPc.

The overall solar cell parameters for all p3HT/PBI3 bilayer devices are summarized in Table 1.

Table 1. Photovoltaic characteristics of different p3HT/PBI3 bilayer photovoltaic devices.

Device	p3HT solvent	PBI3 [wt-%]	PBI3 annealing	V_{OC} [mV]	I_{SC} [µAcm^{-2}]	FF	η_{600nm} [%]
A	PhCl	3.0	-	412	3.64	0.50	0.203
A post-annealed	PhCl	3.0	120 °C, 0.5 h	395	3.29	0.423	0.145
B	PhCl	1.0	-	448	0.43	0.348	0.016
C	*o*-xylene	3.0	-	404	2.31	0.638	0.161
D	*o*-xylene	3.0	120 °C, 1 h	57	0.36	0.330	0.002

The best performing bilayer device was device A with a peak EQE performance of 2.2 % at 555 nm (Fig. 8a). Current-voltage characteristics of these devices were obtained at 600 nm and illumination intensity of ~0.0375 mW/cm^2. Thus device A delivers a short-circuit current density (J_{SC}) of 3.64 µAcm^{-2}, an open-circuit voltage

(U_{OC}) of 412 mV, a fill factor (*FF*) of 0.50 and a power conversion efficiency (η) of 0.203 % (Fig. 8b). This best performing device was post-annealed at 120 °C for 30 minutes. The annealing process results in similar EQE, J_{SC} and U_{OC} values but the fill factor decreases from 0.50 to 0.423 upon annealing (Fig. 8).

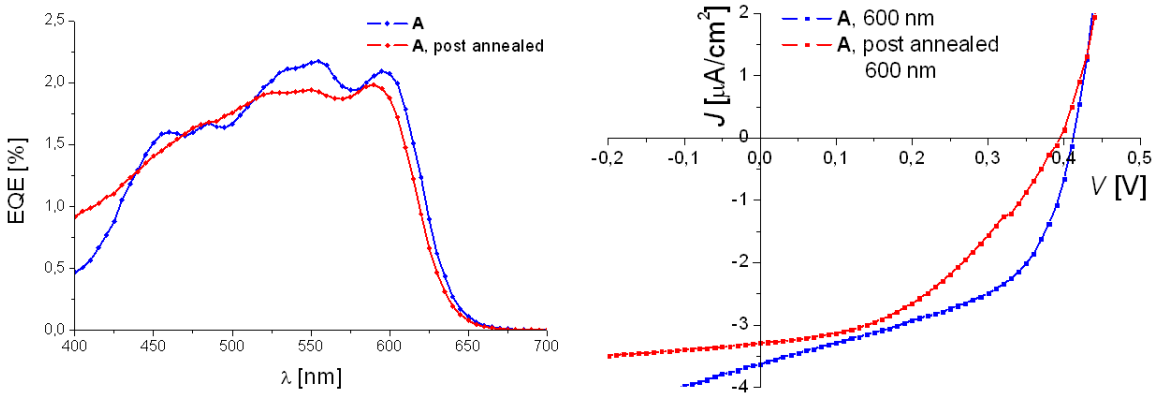

Figure 8. (a) External quantum efficiency for p3HT/PBI3 bilayer device A before and after annealing at 120 °C. (b) Plot of current density (*J*) versus voltage (*U*) under illumination at 600 nm (~0.0375 mW/cm^2) of device A, before and after annealing at 120 °C

For device B a thinner PBI3 layer was investigated. This resulted in a dramatic decrease in device efficiency (Fig. 9).

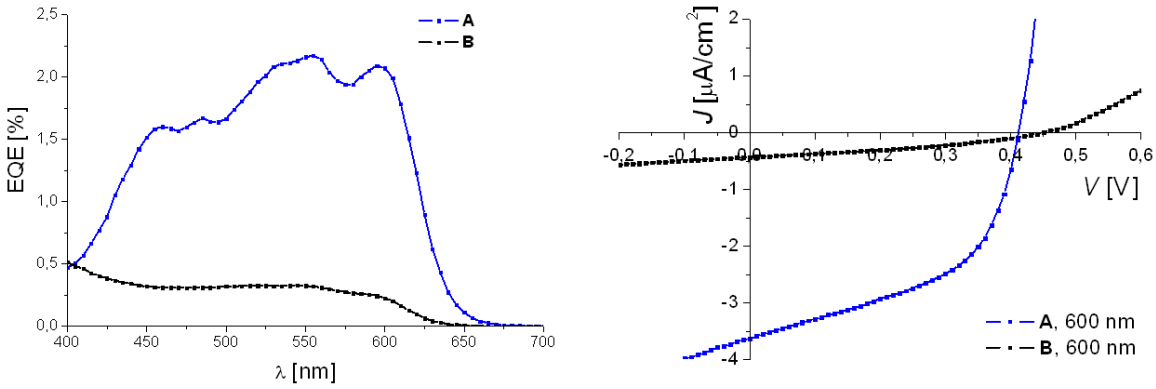

Figure 9. (a) External quantum efficiency for p3HT/PBI3 bilayer device A and B. (b) Plot of current density (*J*) versus voltage (*U*) under illumination at 600 nm (~0.0375 mW/cm^2) of device A and B.

Generally all devices with an annealed PBI3 layer were not operating. Only for devices C and D a comparison between annealed and as spun devices can be drawn. Here the p3HT film was spin casted from *o*-xylene solution. This resulted in an increased fill factor for device C, but a smaller current compared to device A

(chlorobenzene). Thus device C delivers a short-circuit current density (J_{SC}) of 2.31 μAcm^{-2}, an open-circuit voltage (U_{OC}) of 404 mV, a fill factor (*FF*) of 0.64 and a power conversion efficiency (η) of 0.161 %. The annealing process at 120 °C of the PBI3 film before electrode deposition resulted in a dramatically decreased device performance of device D (Fig. 10). This indicates a rearrangement of PBI3 columns.

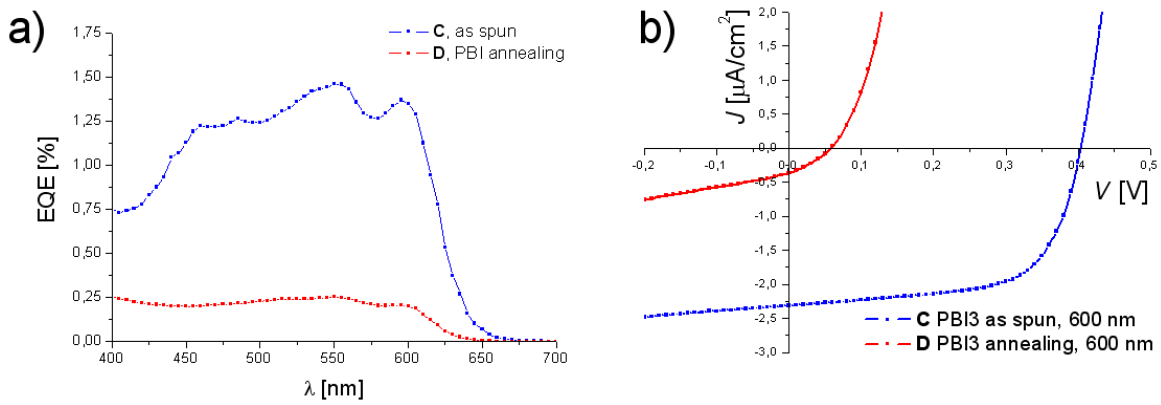

Figure 10. (a) External quantum efficiency for p3HT/PBI3 bilayer device C and D. (b) Plot of current density (*J*) versus voltage (*U*) under illumination at 600 nm (~0.0375 mW/cm^2) of device C and D.

2.4 Experiments on p3HT Col$_h$ blend heterojunction devices

Photoinduced charge separation in general has already been reported in crystalline perylene bisimide - hole conductor polymer blend systems.[6,7,8] By employing crystalline PBI in blends with p3HT *Shin* et al already have realized bulk heterojunction solar cells. The highest efficiency η = 0.18 % (under AM 1.5 conditions) was obtained for a 4:1 PBI:p3HT blend ratio.[8] Thus we have chosen crystalline PBI1 as reference substance and the same device preparation conditions as described. In these experiments devices of the following architecture were prepared: ITO/PEDOT:PSS/PBI:p3HT blend/LiF/Al (Figure 11a). The blends were spin coated from 25 mg/mL *o*-dichlorobenzene (*o*DCB) solutions and used after annealing in the liquid crystalline mesophase or as spun. Figure 11b shows the hypothesized energy diagram of such a device with the corresponding HOMO/LUMO values of the materials.

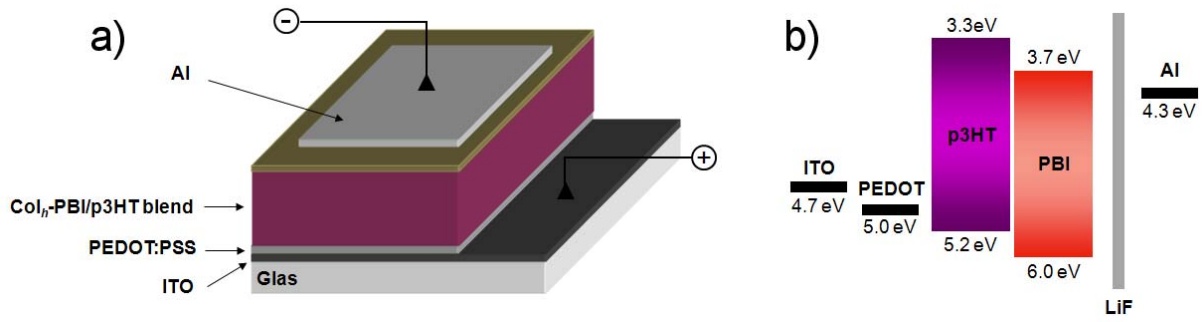

Figure 11. (a) Device architecture for p3HT:PBI blend devices. **(b)** Hypothesized energy diagram of ITO/PEDOT:PSS/p3HT:PBI blend/LiF/Al devices.

The UV-vis absorption spectra of the blend films under investigation are given in Figure 12. The absorption maxima of Col$_h$ PBI2 in the 1:1 and 4:1 PBI2:p3HT blends is at 511 nm. In contrast, the absorption maxima of crystalline PBI1 in the 4:1 PBI1:p3HT blend is shifted hypsochromically by 13 nm to 498 nm.

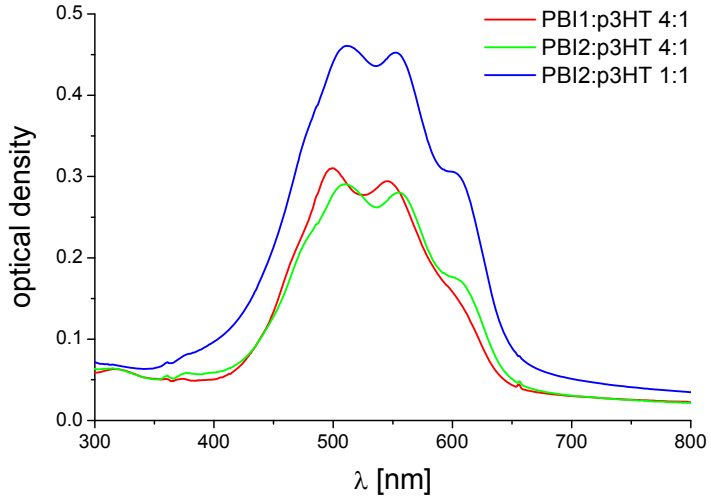

Figure 12. UV-vis absorption spectra of PBI1 or PBI2:p3HT blend films.

A comparison of the AFM-height images of the respective 4:1 PBI:p3HT blend ratios (Fig. 13) also reveals a completely different morphology of these films. For PBI1:p3HT 4:1 film a relatively smooth surface with a good distribution of both materials can be observed, whereas for the PBI2:p3HT 4:1 film a pronounced surface roughness together with a layered morphology can be observed.

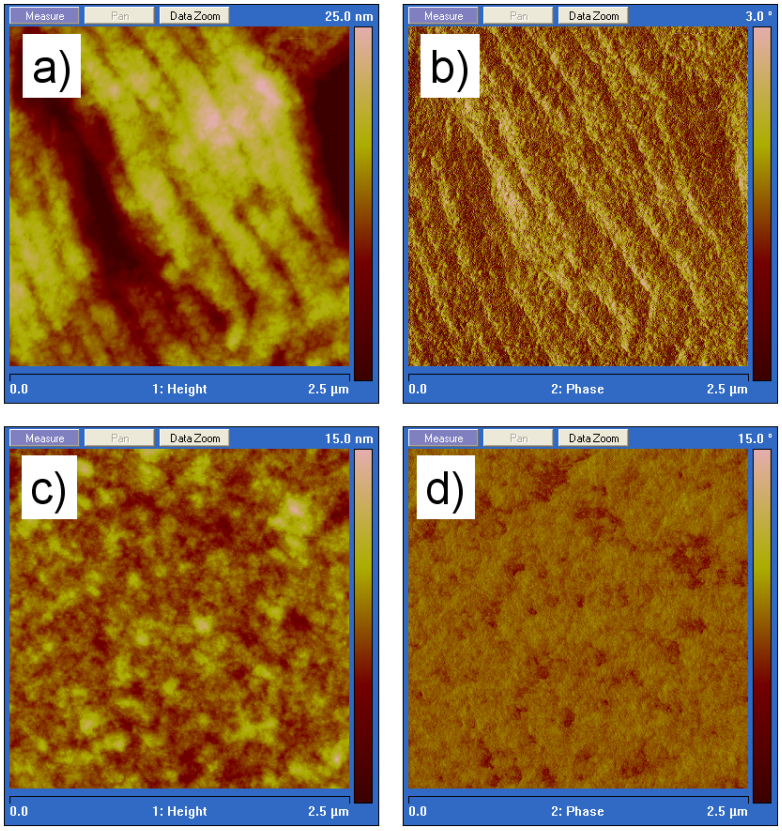

Figure 13. (a) AFM height image of PBI2:p3HT 4:1 blend and (b) corresponding phase image. (c) AFM height image of PBI1:p3HT 4:1 blend and (d) corresponding phase image.

The results of photovoltaic devices with these active layers are summarized in Table 2. The reference devices with PBI1 are working significantly better. For the annealed PBI1:p3HT blend deviceA a peak EQE performance of 7.10 % at 485 nm (Fig. 14a) was obtained. Whereas for annealed devices using PBI2 significantly reduced EQEs with 5.82 % for the 1:1 blend and 0.62 % for the 4:1 blend where observed (Fig. 15a, 16a). Current-voltage characteristics of these devices were obtained under illumination with white light (AM 1.5 spectral conditions, 100 mWcm^{-2}). Thus device E delivers a short-circuit current density (J_{SC}) of 0.664 mAcm^{-2}, an open-circuit voltage (U_{OC}) of 414 mV, a fill factor (*FF*) of 0.46 and a power conversion efficiency (η) of 0.126 % (Fig. 14b).

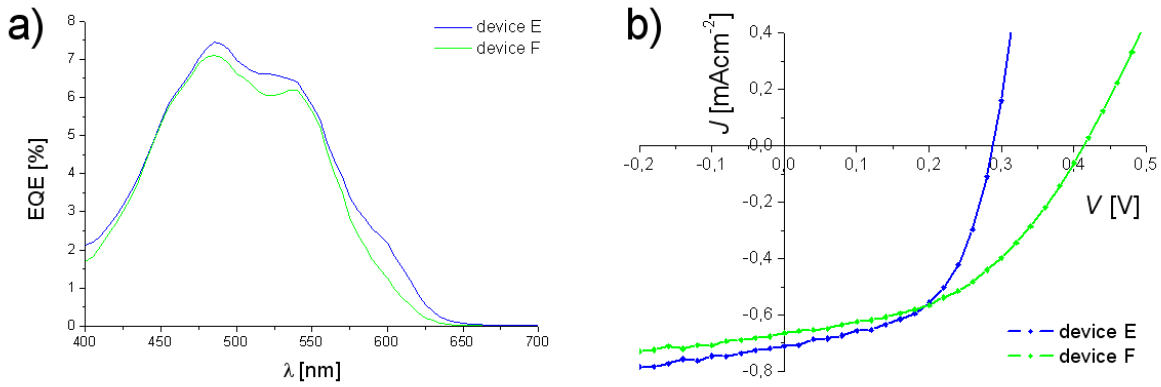

Figure 14. (a) External quantum efficiency for PBI1:p3HT 4:1 blend devices E and F. (b) Plot of current density (*J*) versus voltage (*U*) under illumination with white light (AM 1.5 spectral conditions, 100 mWcm^{-2}) of device E and F.

Current-voltage characteristics (Fig. 15b, 16b) for devices with PBI2 show reduced current and also reduced fill factors, indicating a high resistance in the device. As the electronic properties of both PBI derivatives are similar, this effect can be attributed to a difference in morphology of the active layer of these devices.

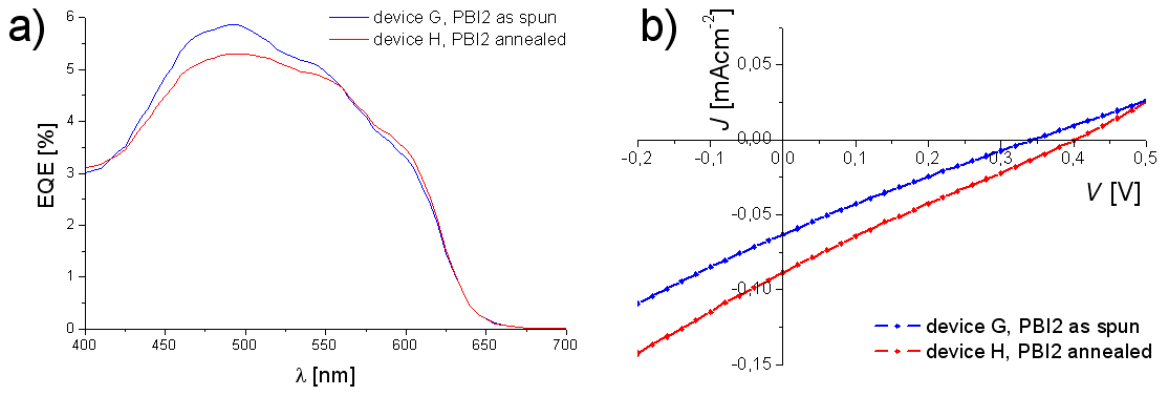

Figure 15. (a) External quantum efficiency for PBI2:p3HT 1:1 blend devices G and H. (b) Plot of current density (*J*) versus voltage (*U*) under illumination with white light (AM 1.5 spectral conditions, 100 mWcm^{-2}) of device G and H.

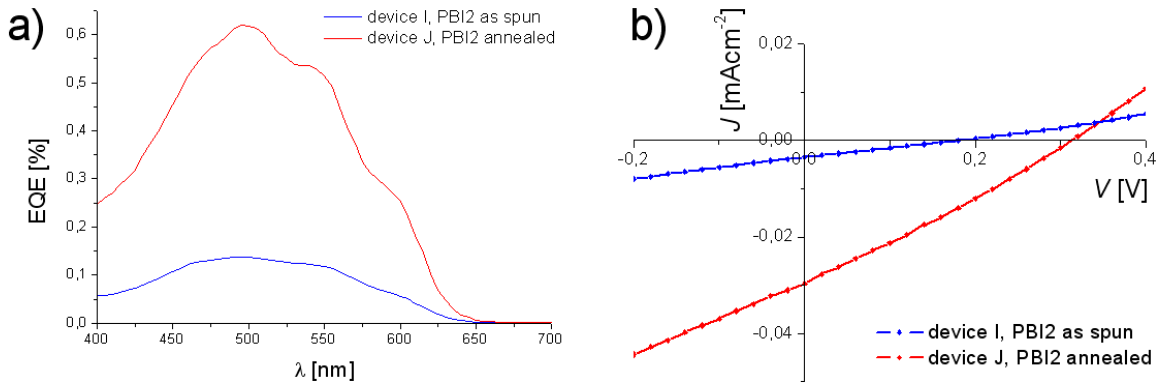

Figure 16. (a) External quantum efficiency for PBI2:p3HT 4:1 blend devices I and J. (b) Plot of current density (*J*) versus voltage (*U*) under illumination with white light (AM 1.5 spectral conditions, 100 mWcm^{-2}) of device I and J.

Table 2. Photovoltaic characteristics of different PBI/p3HT blend devices.

Device	PBI	PBI:p3HT	annealing	V_{OC} [mV]	I_{SC} [mAcm^{-2}]	FF	η [%]
E	PBI1	4:1	as spun	288	0.710	0.541	0.111
F	PBI1	4:1	140 °C, 10 Min	414	0.664	0.457	0.126
G	PBI2	1:1	as spun	343	0.063	0.234	0.005
H	PBI2	1:1	140 °C, 10 Min	400	0.089	0.237	0.008
I	PBI2	4:1	as spun	181	0.0034	0.251	0.0003
J	PBI2	4:1	140 °C 10 Min	313	0.030	0.254	0.002

3. OFETs employing Col$_h$-PBI

Air-stable *n*-type materials are one of the critical material requirements in the field of organic electronics. In contrast to hole conducting materials (*p*-type), very few *n*-type materials are known which offer good electron transport properties in combination with high work function electrodes such as gold. Additionally, highly soluble, solutionprocessable materials are prerequisites for plastic electronics.[9] If a column is to span the gap between two electrodes, its axis must be perpendicular to the electrode surfaces with a face-on arrangement of the individual disks, which means an edge-on arrangement of the columns on the OFET substrate (Fig. 1).

In the following we wanted to investigate the potential of the discotic perylene bisimide PBI2 in OFETs employing different device-configurations (Fig. 17). For the alignment of the discotic molecules, different polarities of the dielectric surface in combination with different thermal annealing procedures of the PBI2 layer were tested.

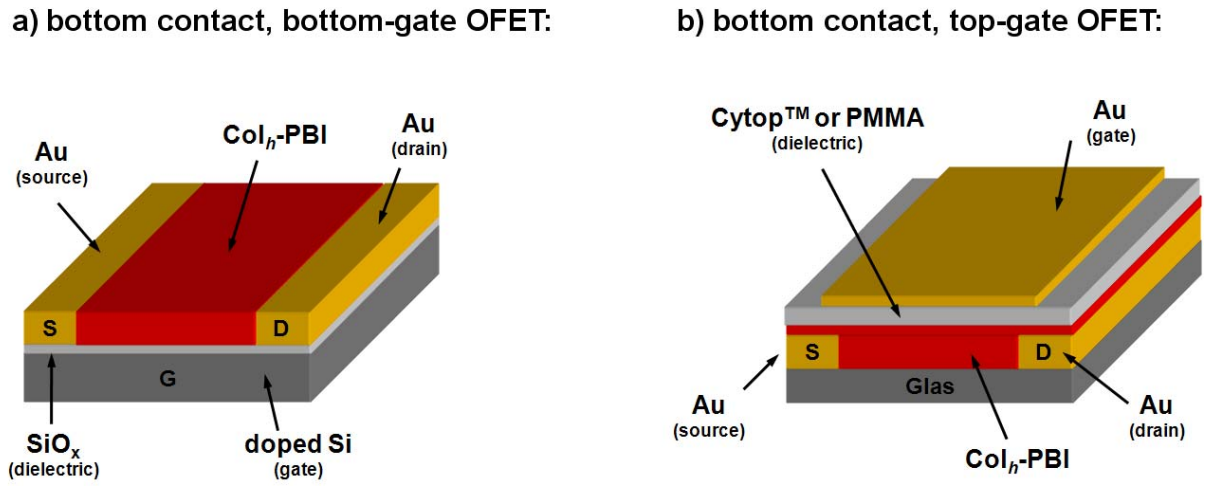

Figure 17. Field effect transistor configurations used: a) bottom contact, bottom-gate; b) bottom contact top-gate.

3.1 Bottom contact, bottom-gate transistors

For bottom contact, bottom-gate transistors (Fig. 17a) we used heavily *n*-doped silicon wafers with a common gate contact carrying 300 nm thermally grown gate oxide layer as transistor substrates. The source and drain contacts were lithographically patterned Au interdigitating electrodes (Channel width, 10 mm ; channel length: 2, 5, 10 and 20 μm). The substrates were cleaned and exposed to

hexamethyldisilizane (HMDS) vapor for approximately 3 h in order to silanize the substrates, rendering the dielectric surface hydrophobic, or exposed to oxygen plasma in order to render the dielectric surface hydrophilic. After HMDS exposure, the substrates were rinsed with isopropanol. PBI2 was spin cast from 1.0 wt-% chloroform solution. This procedure and all subsequent device annealing steps were carried out in a glove box in inert gas. The devices were characterized as spun, after annealing in the liquid crystalline mesophase at 140 °C for 1 h or after melting the sample in the isotropic phase at 170 °C followed by annealing in the mesophase at 140 °C for 1 h. The transistors were characterized in a glove box in inert gas using a HP4155A semiconductor parameter analyzer.

During the annealing process a strong dewetting effect of PBI2 on the hydrophobic OTS surface was observed. Figure 2a shows the transfer characteristics of PBI2 on a hydrophobic dielectric surface comparing the different thermal annealing conditions (obtained for the 2 μm channel). The best performing transistor was obtained after melting the sample in the isotropic phase followed by annealling in the liquid crystalline mesophase at 140 °C. Figure 18b represents the output characteristics of the melted sample. Due to the small channel effect no saturation is observable. The saturation mobilities (μ_{sat}) of PBI2 were extracted from the transfer characteristics by using equation (1) and are summarized in Table 3.[10]

— (1)

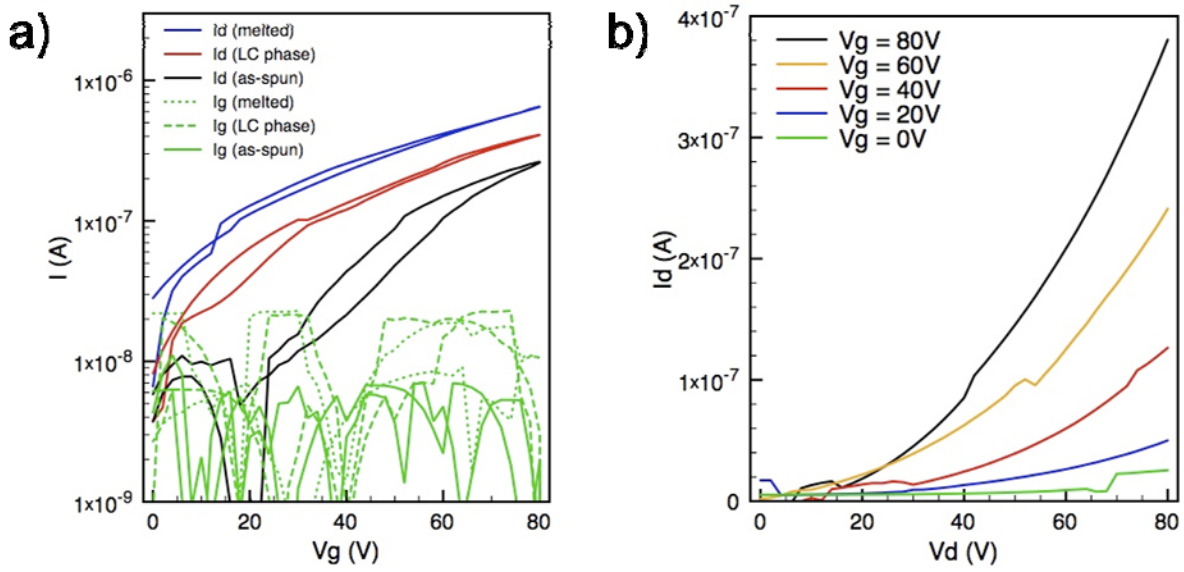

Figure 18. a) Transfer characteristics of PBI2 comparing different thermal annealing conditions. b)

Output characteristics for the melted sample. All measurements were obtained for the 2 μm channel and with a hydrophobic OTS dielectric surface.

Table 3. Saturation mobilities of PBI2 obtained after different thermal annealing procedures.

	as spun	LC phase	melted
saturation mobility μ_{sat} $[cm^2V^{-1}s^{-1}]$	$1.3x10^{-6}$	$1.7x10^{-6}$	$2.6x10^{-6}$

3.2 Bottom contact, top-gate transistors

For bottom contact, top-gate transistors (Fig. 17b) glass substrates with source and drain contacts which were lithographically patterned Au interdigitating electrodes (Channel width, 10 mm ; channel length: 2, 5, 10 and 20 μm) were used. The substrates were either treated with oxygen plasma for a hydrophilic surface or a self-assembled monolayer (SAM) of OTS was used to obtain a hydrophobic surface. To this end, the substrates were exposed to octadecyltrichlorosilane vapour for approximately 2 h. PBI2 was spin cast from 15 mg/mL *o*DCB solution. After annealing of the devices, the dielectric, either PMMA or Cytop™ was processed on top by spin coating and Au gate-electrodes were deposited. The transistors were characterized in a glove box in inert gas using a HP4155A semiconductor parameter analyzer.

For bottom contact, top-gate transistors no transistor characteristics could be obtained, as the layer of highly soluble PBI2 was dissolved during processing of the dielectric. This led to an intermixing of the dielectric and PBI2 interface. For the OTS treated substrates also a strong dewetting of the PBI2 during annealing at high temperatures was observed.

5. Literature

[1] A. Wicklein, S. Gosh, M. Sommer, F. Würthner, M. Thelakkat, *ACS Nano*, **2009**, *3*, 1107-1114.

[2] H.-G. Löhmannsröben, H. Langhals, *Appl. Phys. B*, **1989**, *48*, 449–452.

[3] S. G. Liu, G. Sui, R. A. Cormier, R. M. Leblanc, B. A. J. Gregg, *Phys. Chem. B*, **2002**, *106*, 1307–1315.

[4] A. Wicklein, A. Lang, M. Muth, M. Thelakkat *Journal Of The American Chemical Society,* in preparation.

[5] C. D. Simpson, J. Wu, M. D. Watson, K Müllen, *J. Mater. Chem.*, **2004**, *14*, 494–504.

[6] J. J. Dittmer, E. A. Marseglia, R. H. Friend, *Adv. Mater.* **2000**, *12*, 1270 - 1274.

[7] A. J. Breeze, A. Salomon, D. S. Ginley, H. Tillmann, H.-H. Hörhold, B. A. Gregg, *Appl. Phys. Lett.* **2002**, *81*, 3085 - 3087.

[8] W. S. Shin, H.-H. Jeong, M.-K. Kim, S.-H. Jin, M.-R. Kim, J.-K. Lee, J. W. Lee, Y.-S. Gal, *J. Mater. Chem.* **2006**, *16*, 384 – 390.

[9] S. Hüttner, M. Sommer, M. Thelakkat, *Appl. Phys. Lett.*, **2008**, *92*, 093302.

[10] J. Zaumseil, H. Sirringhaus, *Chem. Rev.*, **2007**, *107*, 1296-1323.